Magneto-optical and dielectric properties of the $C_{20}@C_{60}@(8,8)$ peapod with and without spatial dispersion

E. Rostampour*
Young Researchers and Elites club, Science and Research Branch, Islamic Azad University, Tehran, Iran

Abstract

In this scenario, the dielectric properties of single-wall carbon nanotubes encapsulating onions, so-called onions peapods, is investigated theoretically with and without spatial dispersion. Our results show that the zz element of the energy-loss tensor has the most value when the electric field is in the direction z. The dielectric tensor is different in the case of with and without spatial dispersion. The strongest reflective index is centered at 7.8 eV with spatial dispersion. The Circular dichroism and birefringence coefficient of the $C_{20}@C_{60}@(8,8)$ peapod are of the order of 10^{-4}. Our results show that the optical properties strongly depend on their diameter and chirality. Also, we discuss the relevance of our results for the C_{60} fullerens and single-wall carbon nanotubes.

1. Introduction

Fullerene peapods, discovered by Smith et al. [1], are a typical example of a one-dimensional crystal formed inside single-wall carbon nanotubes (SWNTs). This new solid have interesting electronic [2-4] and optical [5] properties because of the mixed dimensionality. Peapods structural analysis can be performed on a small number of tubes (and even on a single tube), using transmission electron microscopy [6, 7] or electron diffraction [8, 9], or on macroscopic assemblies, using Raman spectroscopy [10-12] or X-ray scattering [12-14]. In the case of organic molecules, as well as fullerenes, π-orbital overlap should lead to new interesting properties. Indeed, in the case of C_{60} peapods, theoretical calculations indicate a large modification of π-electron states of C_{60} due to the hybridization of π orbitals of C_{60} and nearly free electron states of SWNTs [15]. Under electron irradiation [16,17] or thermal treatment under pressure [18], it has been seen experimentally that the fullerene molecules fuse and rearrange to form an inner tube. The encapsulation process is easily

understood on thermodynamic grounds, being driven by van der Waals attractions which are maximized when the fullerenes are inside the nanotube and regularly spaced [19]. The highly symmetrical structure of carbon onions suggests that this material has unique properties with various significant potential applications. The structural stability of carbon nano-onion $C_{20}@C_{60}@C_{240}$ has been investigated by performing molecular dynamics computer simulations. Calculations have been realized by using an empirical many-body potential energy function for carbon [20]. Spherical and icosahedral nanoparticles have studied theoretically using various models. The smallest possible cage structure of carbon, C_{20}, the most stable cage structure of carbon at room temperature, C_{60}, and the onion-like structure of these two carbon nanoballs, $C_{20}@C_{60}$, is considered in the present theoretical study. The rest of the paper is arranged as follows. In Sec. 2, we present our calculation methods. In Sec. 3, calculation results presented and discussed in detail the dielectric properties of $C_{20}@C_{60}@(8,8)$. Finally, a short synopsis will be given in Sec. 4.

2. Theoretical model

The Hamiltonian of a n-atom fullerene C_n or (n,n) carbon nanotube is described in the tight-binding (TB) approximation with one π orbital per site [21, 22]

$$H_n = -t_n \sum_{<i,j>,\sigma} (c_{i\sigma}^{\dagger} c_{j\sigma} + H.c.) . \quad (1)$$

where $c_{i\sigma}^{\dagger}(c_{i,\sigma})$ is the creation (annihilation) operator of the π electron at the site i with spin σ, the sum is taken over nearest-neighbor pairs $< i,j >$. Also, t_n is hopping integral between nearest neighbor ith and jth sites of the ideal system. It is worth recalling that a simple tight-binding Hamiltonian for π orbitals reproduces extremely well the order and degeneracies of electronic levels near the Fermi energy as obtained in more sophisticated molecular orbital calculation. The tight-binding Hamiltonian for onions peapods becomes that of the isolated layers with an inter-layer interaction term

$$H_{\text{onions peapods}} = \sum_n^N H_n + t_{\perp} \sum_{<ij>} (c_i^{\dagger} c_j + c_j^{\dagger} c_i) \quad (2)$$

where site i belongs to a inner tube, and site j is its NN or NNN on the adjacent outer layer and $t_{\perp}$ is the hopping between pairs of the NN and NNN between layers [23]. For the determination of the complex optical dielectric tensor ε_{ij} , we obtain the element of the internal or local field coefficients using local field and Ewald method that it fully described in Ref. [24-27]. In the principal dielectric axis of the $C_{20}@C_{60}@(8,8)$ peapod, we can define the complex refractive index as,

$$N_\delta(\omega,\vec{k},\vec{B}) = [n_\delta(\omega,\vec{k},\vec{B}) + ik_\delta(\omega,\vec{k},\vec{B})] = \sqrt{\varepsilon_\delta(\omega,\vec{k},\vec{B})}$$
(3)

where $\varepsilon_\delta(\omega,\vec{k},\vec{B})$ is the complex dielectric function of the δth principal dielectric axis, $n_\delta(\omega,\vec{k},\vec{B})$ is the real part of the refractive index and $k_\delta(\omega,\vec{k},\vec{B})$is the imaginary part of the refractive index. Also, the reflectivity of the $C_{20}@C_{60}@(8,8)$ peapod is given by,

$$R_\delta = \frac{|1-N_\delta(\omega,\vec{k},\vec{B})|^2}{|1+N_\delta(\omega,\vec{k},\vec{B})|^2} = \frac{|1-n_\delta(\omega,\vec{k},\vec{B})|^2+k_\delta(\omega,\vec{k},\vec{B})^2}{|1+n_\delta(\omega,\vec{k},\vec{B})|^2+k_\delta(\omega,\vec{k},\vec{B})^2}$$
(4)

The magneto–optical properties of solids in the presence of the magnetic field $\vec{B}$, are theoretically described by birefringence coefficient, θ, and the circular dichroism, CD. These are given using the terms of real $n_\pm(\omega,\vec{k},\vec{B})$and the imaginary $k_\pm(\omega,\vec{k},\vec{B})$, for left and right polarizations in the plane perpendicular to the magnetic field, by the following equations:

$$\theta(\omega,\vec{k},\vec{B}) = \frac{\omega}{2c}[n_+(\omega,\vec{k},\vec{B}) - n_-(\omega,\vec{k},\vec{B})].$$

and

$$CD(\omega,\vec{k},\vec{B}) = \frac{\omega}{2c}[k_+(\omega,\vec{k},\vec{B}) - k_-(\omega,\vec{k},\vec{B})].$$
(5)

For the magnetic field in the direction z, the real and imaginary parts of refractive indices for left and right polarizations are determined from the following equations:

$$[n_\pm(\omega,\vec{k},\vec{B}) + ik_\pm(\omega,\vec{k},\vec{B})]^2 = \varepsilon_\pm(\omega,\vec{k},\vec{B})$$
(6)

and

$$\varepsilon_\pm(\omega,\vec{k},\vec{B}) = \varepsilon_{xx}(\omega,\vec{k},\vec{B}) \pm \varepsilon_{xy}(\omega,\vec{k},\vec{B})$$
(7)

Here, $\varepsilon_{xx}(\omega,\vec{k},\vec{B})$ and $\varepsilon_{xy}(\omega,\vec{k},\vec{B})$ are the xx and xy elements of dielectric tensor in the presence of a magnetic field, respectively. The frequency and magnetic field-dependent dielectric tensor must be determined for calculating these parameters.

3. Results and discussions

Optical absorption characterization of thin films of nanotubes and peapods has carried out by Kataura et al. [28]. It has been recently shown that individual semiconducting nanotubes can be isolated from bundles in surfactant micelles and show characteristic signatures in UV-vis absorption and

fluorescence spectra [29]. Efforts to isolate peapod samples for optical characterization are still in progress, so the effect of filling on optical behavior of individual nanotubes remains unknown. In order to take into account the effect of the curvature of the shell for the various fullerenes, we consider the hopping parameter t_n to be a function of the mean radius R_n of the (nearly) spherical shell of n C atoms and the mean inter-atomic distance d_n ($t_n = t[1 - \frac{1}{2}\left(\frac{d_n}{R_n}\right)^2]$) [30]. The value t = −2.73 eV is a suitable hopping for graphene. We calculated the mean radius of the shell is the main geometrical variable, with the mean inter-atomic distance being approximately constant and hopping integral for the various fullerenes C_n and carbon nanotube. Our results summarized in Table I.

Carbon nanotube	$d_n(A°)$	$R_n(A°)$	$t_n(eV)$	C_n	$d_n(A°)$	$R_n(A°)$	$t_n(eV)$
(8,8)	1.4211	5.4388	2.64	C_{20}	1.3914	1.9495	2.035
				C_{60}	1.4342	3.4425	2.49

TABLE I: Mean interatomic C-C distances, mean radii and hopping integral for the single-wall icosahedral fullerenes and carbon nanotube.

The calculated real and imaginary parts of the xx, yy and zz elements of the dielectric tensor that are denoted by ε_{ij}^1 and ε_{ij}^2, respectively, are shown in figures 1(a)-1(c) and figures 2(a)-2(c) for the C_{20}@C_{60}@(8,8) peapod with (Real[CK]= Real [CK_x]= Real [CK_y]= Real [CK_z]=2 eV) and without spatial dispersion. Our calculations indicate that the $\varepsilon_{xx}(\omega, \vec{K}, \vec{B})$ and $\varepsilon_{yy}(\omega, \vec{K}, \vec{B})$ spectra are almost same and are different with $\varepsilon_{zz}(\omega, \vec{K}, \vec{B})$ spectra. Then, the dielectric tensor elements vary depending on the C_{20}@C_{60}@(8,8) peapod orientation relative to the electric field of light. We calculated the average imaginary ($\varepsilon_{av}^1, \varepsilon_{av} = \frac{\varepsilon_{xx}+\varepsilon_{yy}+\varepsilon_{zz}}{3}$) and real ($\varepsilon_{av}^2$) parts of the elements of the dielectric tensor and our results are shown in figures 1(d) and 2(d). The imaginary part of the dielectric tensor could exhibit the pronounced peaks at the specific frequencies, as shown in Figs. 2(a)–(d). Such peaks are due to the single-particle excitations of the band-edge states. On the other hand, the real part of the dielectric tensor exhibits drastic changes there. The intertube atomic overlaps, which lead to the overlaps of valence and conduction bands, account for the complicated excitation spectrum. In Figs. 1(a)-1(c), the first peak of the dielectric tensor centered at $\omega = 1.03$ (1.33), 1.03(1.33) and 2.04(1.33) eV for the C_{20}@C_{60}@(8,8) peapod without (with) spatial dispersion when the electric field is in the directions x, y and z, respectively. Our results show that the zz element of the dielectric tensor has the lowest value when the electric field is in the direction z. In the imaginary part of the dielectric tensor the observed peaks indicate the direct interband

transitions between the Van Hove singularities of the density of states. The loss function measured in an electron energy-loss spectroscopy experiment is a direct probe of the collective excitations of the system under consideration. Thus, by definition, all peaks in the measured loss function should be considered as plasmons. These peaks can, however, have different origins such as charge carrier plasmons, interband or intraband excitations. From the *q*-dependence of the loss function, one can distinguish directly between features arising from localized or delocalized electronic states. Localized states give rise to a vanishingly small dispersion of peaks in the loss function as has been observed, for example, for the features related to the interband excitations and both the π and $\pi + \sigma$ plasmons of C_{60} [31]. On the other hand, excitations between delocalized states generally exhibit a band structure dependent dispersion relation. Bearing these points in mind, the identification of excitations between localized and delocalized states in SWNTs is straightforward. Thus, in combination with the well-known one-dimensionality of nanotubes the nondispersive peaks in the loss function can be attributed to excitations between localized states polarized *perpendicular* to the nanotube axis and thus resemble molecular interband transitions such as those of C_{60}. In contrast, the π-plasmon (at 5.2 eV for low **q**), represents a plasma oscillation of delocalized states polarized *along* the nanotube axis. The dispersion relations of both the π and the $\pi + \sigma$ plasmons in SWNTs and graphite are very similar, which confirms the graphitic nature of the axial electron-system in carbon nanotubes. The energy-loss tensor ($= Im[-\frac{1}{\varepsilon_{ij}(\omega)}]$) for the $C_{20}@C_{60}@(8,8)$ peapod is shown in Figs. 3(a)-(d). There are very sharp structures in the energy –loss tensor corresponding to the energy locations where $\varepsilon(\omega)$ vanishes. In Fig. 3(d), the major structures of spectrum are centered at1.63, 3.34, 3.6, 4.26, 5.25, 6.98 and 7.99 eV without spatial dispersion. Also, the major structures of spectrum are centered at 1.54, 3.10, 4.97, 6.74 and 7.64 eV with spatial dispersion in Fig. 3(d). The broader peak centered at 6.98 (6.74) eV without (with) spatial dispersion are also evident. These peaks can be fitted by a Gaussian form with a full width at half maximum 0.5 eV. These broad peaks may come from a collective excitation of the layered electronic charges of the $C_{20}@C_{60}@(8,8)$ peapod. Our results show that the zz element of the energy-loss tensor has the most value when the electric field is in the direction z. The optical transitions are extremely well defined and intense due to the presence of van Hove singularities in the density of states for both the occupied and unoccupied states. Also, the optical transition energies strongly depend on the nanotube type (metallic or semiconducting) and helicity(or diameter). . Pichler et al. [32] measured the loss function of purified SWNTs for various momentum transfers q and low excitation energies. The spectra show peaks

corresponding to excitation from the valence bands to the conduction bands as well as plasmon peaks. The latter are at 5.2 eV (π-plasmon) and 21.3 eV ($\pi + \sigma$-plasmon), somewhat lower compared to the corresponding values for graphite (6 and 27 eV) because of curvature effects in nanotubes. The π- and $\pi + \sigma$-plasmons show strong dispersion (dependence on the wavevector q). The peaks observed at 0.85, 1.45, 2.0 and 2.55 eV are dispersionless and can be attributed to $\pi - \pi^*$ interband transitions of different nanotubes. For dipole transitions, these energies are equal to the separation between the mirror spikes of the electronic DOS. Using theoretical predictions for the electronic band structure of the nanotubes, the observed peaks can be assigned to nanotubes with certain diameters and chiralities [33]. We next calculate the refractive index and reflectivity with the obtained dielectric tensor for $C_{20}@C_{60}@(8,8)$ peapod using the mentioned model. Figures 4(a)-(b) represent the refractive index and reflectivity, respectively. We have the strongest reflective index at low energy (in $\omega = 1.32(1.02)$ eV) and diminution in the oscillator strengths of peaks with increasing energy with (without) spatial dispersion. Using Equation (5), we have calculated the Circular dichroism and birefringence coefficient for non-zero magnetic field. Figure 5 represents the Circular dichroism and birefringence coefficient for the magnetic field in the direction z with strength equal to 2T. Circular dichroism and birefringence coefficient are of the order of 10^{-4} for the $C_{20}@C_{60}@(8,8)$ peapod. In general, the optical conductivity of these sp^2 conjugated carbon systems show peaks due to transitions between the (π/σ) and the (π^*/σ^*) electronic states. In C_{60} these peaks are very pronounced which is consistent with the high symmetry of the molecule and the weak, van der Waals interactions in the solid state [34], making C_{60} a prototypical zero-dimensional solid. In graphite three broad features are observed at 4.56 ± 0.05, 13 ± 0.05, and 15 ± 0.05 eV. Their breadth is an expression of the bandlike nature of the electronic states in the graphite plane. For the SWNTs we also find three broad features at energies slightly lower than those in graphite-i.e. 4.3 ± 0.1, 11.7 ± 0.2, and 14.6 ± 0.1 eV. Importantly, the optical conductivity of the SWNTs also exhibits additional structures at low energy [35].

4. Concluding remarks

Based on the TB Hamiltonian, we studied in detail the dielectric properties of $C_{20}@C_{60}@(8,8)$ peapod. The theoretical results are well consistent with the numerical observations. The size, geometry and spatial dispersion affect the dielectric properties. Carbon nanotubes support both excitations between delocalized and localized electronic states. The π-plasmon exhibits significant q-dependence, with a dispersion relation similar to that of the graphite plane, demonstrating the graphitic nature of the nanotube electron system along the tube axis. The intertube atomic overlaps would largely reduce the plasmon strength, produce more plasmon modes, and make acoustic plasmons change into optical

plasmons. The optical plasmons are directly related to free holes in valence bands and free electrons in conduction bands. Our results show that the strongest reflective index centered at low energy.

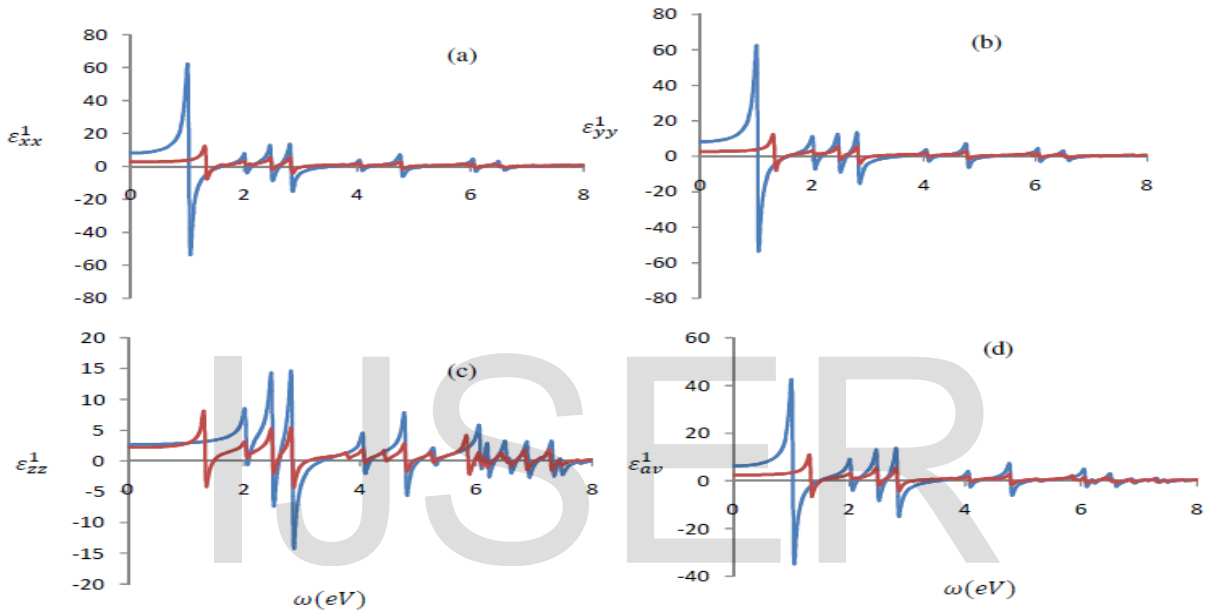

Figure 1. Calculated real part of the (a) xx, (b) yy, (c) zz elements of the dielectric tensor, and (d) average of the dielectric tensor for the $C_{20}@C_{60}@(8,8)$ peapod without spatial dispersion(Real [CK]=0.0 eV) and with spatial dispersion (Real[CK]=2.0 eV).

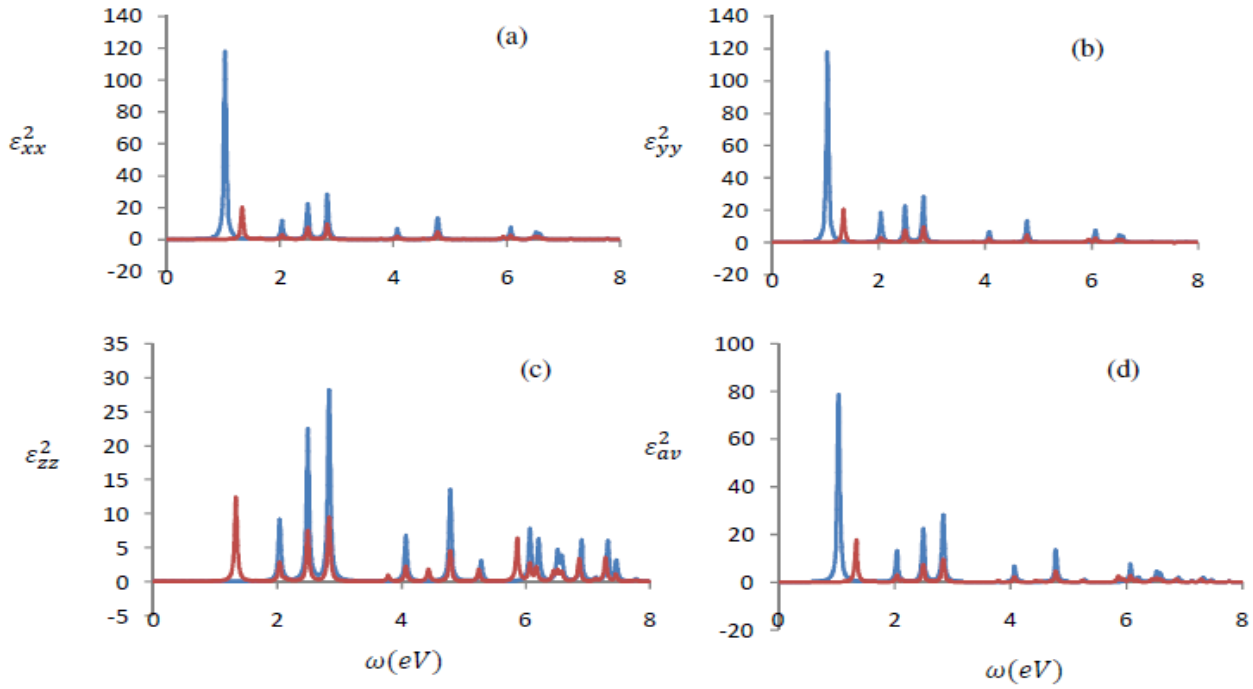

Figure 2. Calculated imaginary part of the (a) xx, (b) yy, (c) zz elements of the dielectric tensor, and (d) average of the dielectric tensor for the $C_{20}@C_{60}@(8,8)$ peapod without spatial dispersion(Real [CK]=0.0 eV) and with spatial dispersion (Real[CK]=2.0 eV).

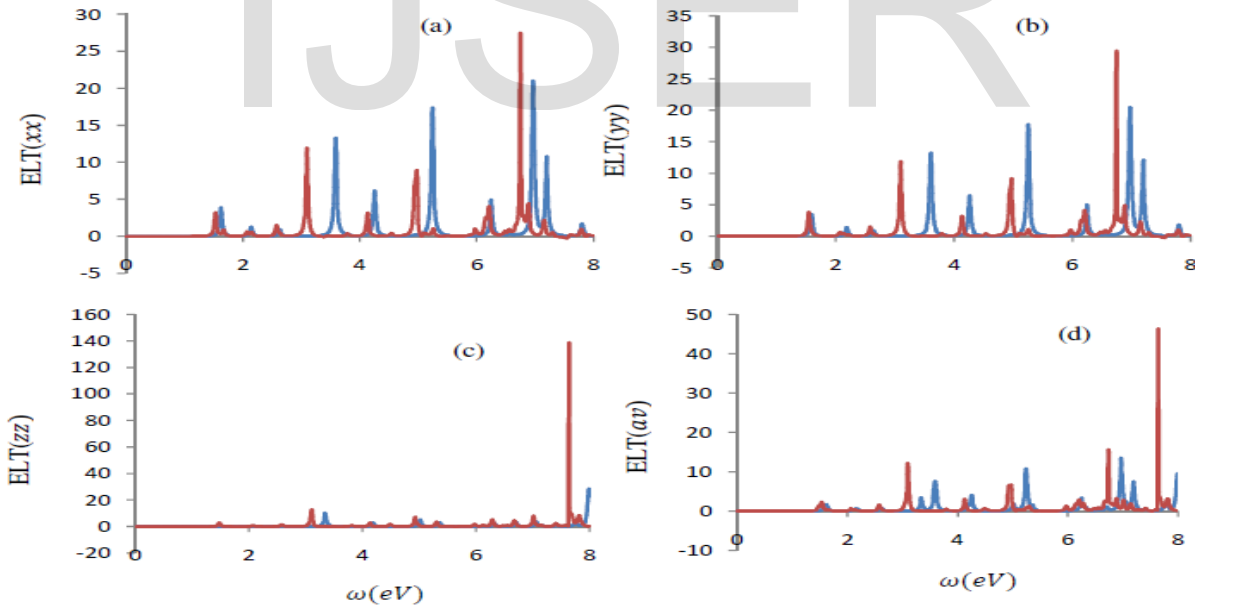

Figure 3. The (a) xx, (b) yy, (c) zz elements of the energy-loss tensor, and (d) average of the energy loss tensor for the $C_{20}@C_{60}@(8,8)$ peapod without spatial dispersion(Real [CK]=0.0 eV) and with spatial dispersion (Real[CK]=2.0 eV).

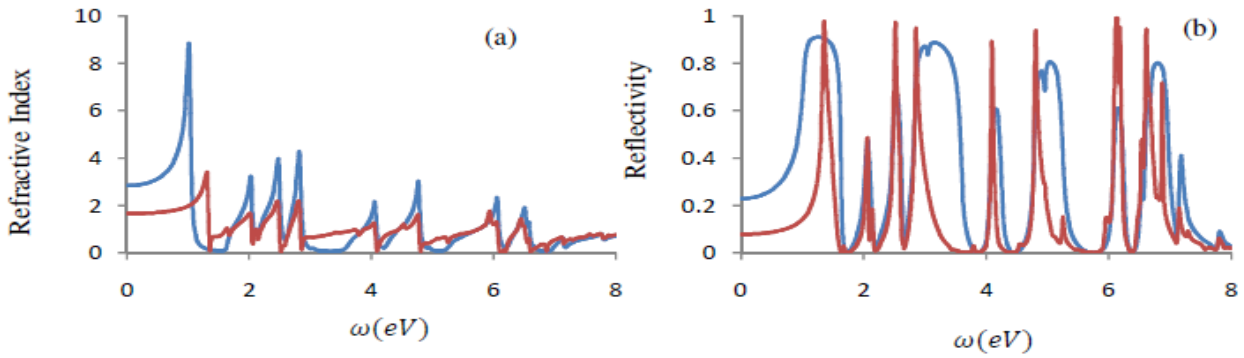

Figure 4. The (a) refractive index and (b) reflectivity of the $C_{20}@C_{60}@(8,8)$ peapod without spatial dispersion (Real [CK]=0.0 eV) and with spatial dispersion (Real[CK]=2.0 eV).

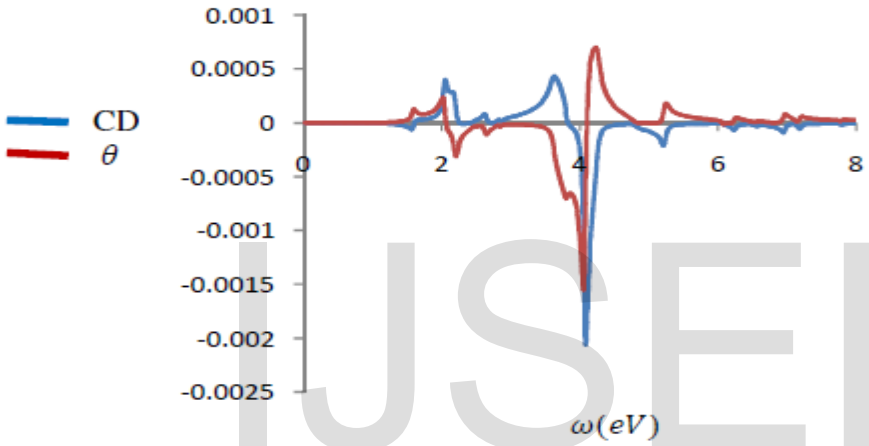

Figure 5. Circular dichroism ( ) and the birefringence coefficient ( ) at magnetic field 2T for the $C_{20}@C_{60}@(8,8)$ peapod.

References

[1] B.W. Smith, M. Monthioux, D.E. Luzzi: Nature **396**, 323 (1998)

[2] S. Saito and S. Okada, Proc. 3rd Symposium on atomic scal surface and interface dynamic (Fukuoka 1999) p.307.

[3] Eliasen A, Paaske J, Flensberg K, Smerat S, Leijnse M, Wegewijs M.R, et al. Transport via coupled states in a C_{60} peapod quantum dot. Phys. Rev. B. 2010;81:155431-1-5

[4] Pichler T, Kukovecz A, Kuzmany H, Kataura H, Achiba Y. Quasicontinuous electron and hole doping of C_{60} peapods. Phys. Rev. B 2003;67:125416-1-7

[5] Kataura H, Maniwa Y, Abe M, Fujiwara A, Kodama T, et al. Optical properties of fullerene and non-fullerene peapods Appl. Phys. A 2002;74:349-354

[6] B.W. Smith, M. Monthioux, D.E. Luzzi, Nature 396 (1998) 323.

[7] H. Kataura, Y. Maniwa, T. Kodama, K. Kikuchi, H. Hirahara, K. Suenaga, S. Iijima, S. Suzuki, Y. Achiba and W. Kr¨atschmer, Synthetic Metals 121 (2001) 1195

[8] X. Liu, T. Pichler, M. Knupfer, M.S. Golden, J. Fink, H. Kataura, Y. Achiba, K. Hirahara and S. Iijima, Phys. Rev. B 65 (2002) 045419,

[9] K. Hirahara, S. Bandow, K. Suenaga, H. Kato, T. Okazaki, H. Shinohara and S. Iijima,Phys. Rev. B 64 (2001) 115420

[10] H. Kataura, Y. Maniwa, T. Kodama, K. Kikuchi, H. Hirahara, K. Suenaga, S. Iijima, S. Suzuki, Y. Achiba and W. Kr¨atschmer, Synthetic Metals 121 (2001) 1195.

[11] H. Kuzmany, R. Pfeiffer, C. Kramberger, T. Pichler, X. Liu, M. Knupfer, J. Fink, H. Kataura, Y. Achiba, B.W. Smith and D.E. Luzzi, Appl. Phys. A 76 (2003) 449,

[12] H. Kataura, Y. Maniwa, M. Abe, A. Fujiwara, T. Kodama, K. Kikuchi, H. Imahori, Y. Misaki, S. Suzuki, Y. Achiba, Applied Physics A, 74 (2002) 349.

[13] Y. Maniwa, H. Kataura, M. Abe, A. Fujiwara, R. Fujiwara, H. Kira, H. Tou, S. Suzuki; Y. Achiba, E. Nishibori, M. Takata, M. Sakata and H. Suematsu, J. ofPhys. Soc. of Japan 72 (2003) 45.

[14] W. Zhou, K. I. Winey, J. E. Fischer, T. V. Sreekumar, S. Kumar, and H. Kataura, Appl. Phys. Lett. 84 (2004) 2172

[15] S. Okada, S. Saito, A. Oshiyama: Phys. Rev. Lett. **86**, 3835 (2001).

[16] Luzzi DE, Smith BW. Carbon 2000;38(11-12):1751-1756

[17] Hernández E, Meunier V, Smith BW, Rurali Rm Terrones H Buongioro Nardelli M et al. Nano Lett 2003;3(8):1037-1042

[18] Bandow S, Takizawa M, Hirahara K, Yudasaka M, Iijima S. Chem Phys Lett 2001;337(1-3):48-54

[19] Hodak M, Girifalco LA. Phys Rev B 2003; 67:075419-1-4

[20] S. Erkocu,*Nano Lett.,* Vol. 2, No. 3, 2002

[21] E. Manousakis, Phys. Rev. B 44, 10991 (1991).

[22] J. Ma and R. K. Yuan, "Electronic and optical properties of finite zigzag carbon nanotubes with and without Coulomb interaction ", Phys. Rev. B 57, 9343 (1998).

[23] D. A. Lovey and R. H. Romer, arXiv:1305.6299v1 [cond-mat.mes-hall] (2013).

[24] E. Rostampour, "The linear optical and magneto-optical susceptibilities and geometric effects of nine La@C_{82} (C_{82}) crystal isomers", J. Appl. Phys. 116, 133104 (2014),

[25] V. M. Agranovich and V L .Ginzburg," *Crystal Optics with Spatial Dispersion and Excitons",* (Berlin: Springer)(1984).

[26] J. Dong, J. Jiang, J. Yu, Z. Wang, and D. Xing, Phys. Rev. B 52, 9066 (1995);

[27] J. Dong, J. Jiang, J. Yu, Z. Wang, and D. Xing, *ibid.* 51, 1997 (1995).

[28] H. Kataura, et al. Appl. Phys. A, 74, 349 (2002); A. Thess, et al. Science, 273, 483 (1996).

[29] M. J. Oconnell, et al. Science, 297, 593 (2002); S. M. Bachilo, et al. Science, 298, 2361(2002

[30] Dresselhaus et al. Science and application of nanotubes, edited by D. Tomarek and R. J. Endbody (Kluwer/Academic/Dordrecht/New York, 2002)

[31] Romberg H, Sohmen E, Merkel M, Knupfer M, Alexander M, et al. "Electronic structure of undoped and doped fullerenes", Synthetic Metals (1993)55–57:3038.

[32] T. Pichler, M. Knupfer, M.S. Golden, J. Fink, A. Rinzler, R.E. Smalley, "Localized and Delocalized Electronic States in Single-Wall Carbon Nanotubes", Phys. Rev. Lett. 80 (1998) 4729

[33] H. Kataura, Y. Kumazawa, Y. Maniwa, I. Umezu, S. Suzuki, Y. Ohtsuka, Y. Achiba, "Optical properties of single-wall carbon nanotubes", Synth. Metals 103 (1999) 2555.

[34] Sohmen E, Fink J. Phys Rev B 1993;47(14):532.

[35] *M. Knupfer* T. Pichler, M.S. Golden, J. Fink, A. Rinzler, R.E. Smalley, "Electron energy-loss spectroscopy studies of single wall carbon nanotubes", *Carbon* 37 (1999) 733 –738 737.